

## Size effects on excitons in nano-rings

Hui Hu<sup>a</sup>, Dai-Jun Li<sup>a</sup>, Jia-Lin Zhu<sup>a,b</sup>, Jia-Jiong Xiong<sup>a</sup>

<sup>a</sup> Department of Physics, Tsinghua University, Beijing 100084, P. R. China

<sup>b</sup> Center for Advanced Study, Tsinghua University, Beijing 100084, P. R. China

(December 2, 2024)

The size effects of an exciton in a nano-ring are investigated theoretically by using an effective-mass Hamiltonian which can be separated in terms of the center-of-mass and relative coordinates. The binding energy and oscillator strength of the ground state are calculated for two different ring radii as a function of the ring width. The resulting linear optical susceptibility of the low-lying exciton states is also discussed. PACS numbers: 73.20.Dx, 71.35.-y, 78.66.Fd

Recent progress in nanofabrication techniques has made it possible to construct self-assembled InGaAs nano-rings [1–5]. Quite different from the previously fabricated sub-micron GaAs quantum rings [6], those nano-rings now achieved are so small (with characteristic inner/outer radius of 20/100 nm and 2-3 nm in height), that the electrons and holes can propagate coherently (non-diffusively) throughout the ring. In this meaning, nano-rings can be viewed as a promising candidate for application in microelectronics as well as the conventional quantum dots. Moreover, the additional non-simply-connected geometry of nano-rings is of inherent interest at the moment [7–11].

While the conventional quantum dots have been investigated theoretically and experimentally in depth [12–16], nano-rings with strong quantum effects have only been recently treated [9,11,17–23]. In particular, the theoretical results related to the quantum confinement effects on *exciton* states in nano-rings are very rare. Only recently did Song and Ulloa report numerical calculations of the binding energy and electron-hole separation of the exciton in an external magnetic field [11]. They claim that the excitons in nano-rings behave to a great extent as those in quantum dots of similar dimensions.

In this paper, we would like to investigate the size effects on excitons of nano-rings by introducing a simplified confining potential, which is applicable to the *realistic* self-assembled semiconducting InGaAs nano-rings achieved to date [2,4,5]. To explore the role of different confinements, we express the model Hamiltonian in terms of the center-of-mass and relative coordinates and calculate binding energies, oscillator strengths and their dependence on the width of nano-rings, as well as the linear optical susceptibility which would be measurable in photoluminescence experiments, for example.

Our model is a two-dimensional exciton in a nano-ring, simulating recent experimental nano-ring structures [2,4,5]. The nano-ring is described by an electron-hole pair ( $i = e, h$ ) with an effective band edge mass  $m_i^*$  mov-

ing in a x-y plane, and a ring-like confining potential is introduced as  $U(\vec{r}_i) = \frac{1}{2R_0^2} m_i^* \omega_i^2 (\vec{r}_i^2 - R_0^2)^2$ , where  $R_0$  is the radius of the ring and  $\omega_i$  is the characteristic frequency of the radial confinement, giving a characteristic ring width  $W \approx 2\sqrt{\frac{\hbar}{2m_i^* \omega_i}}$  for each particle. The resulting model Hamiltonian is thus given by:

$$\mathcal{H} = \sum_{i=e,h} \left[ \frac{\vec{p}_i^2}{2m_i^*} + U(\vec{r}_i) \right] - \frac{e^2}{4\pi\epsilon_0\epsilon_r |\vec{r}_e - \vec{r}_h|}, \quad (1)$$

where  $\vec{r}_i = (x_i, y_i)$  and  $\vec{p}_i = -i\hbar\vec{\nabla}_i$  denote the position vector and momentum operator,  $\epsilon_0$  is the vacuum permittivity, and  $\epsilon_r$  is the static dielectric constant of the host semiconductor. It should be pointed out that the present ring-like confining potential can be rewritten as  $U(\vec{r}_i) = \frac{1}{2} m_i^* \omega_i^2 (r_i - R_0)^2 \frac{(r_i + R_0)^2}{R_0^2}$ . If one replaces the operator  $r_i$  in factor  $\frac{(r_i + R_0)^2}{R_0^2}$  by its mean value  $\langle r_i \rangle = R_0$ , the confining potential returns to the widely used parabolic form [2,11,20,22]. On the other hand, for narrow rings (with steep confinement) our confining potential gives a more realistic description than does the parabolic form. In the latter, as pointed by Song and Ulloa [11], the associated wavefunctions fail in a real system because the increased confinement may push the levels into the anharmonic part of the potential and even produce deconfinement of carriers. Figs. (1a) and (1b) display the shape of the ring potential with two different radii: 10 and 30 nm. The solid and dashed lines correspond to the ring width  $W = 16.7$  and 9.6 nm, respectively.

In terms of the relative coordinate  $\vec{r} = \vec{r}_e - \vec{r}_h$  and center-of-mass coordinate  $\vec{R} = \frac{m_e^* \vec{r}_e + m_h^* \vec{r}_h}{m_e^* + m_h^*}$ , the model Hamiltonian is divided into

$$\begin{aligned} H &= \mathcal{H}_{cm}(\vec{R}) + \mathcal{H}_{rel}(\vec{r}) + \mathcal{H}_{mix}(\vec{R}, \vec{r}), \\ \mathcal{H}_{cm} &= \frac{\vec{P}_{cm}^2}{2M} + \frac{M\omega_{cm}^2}{2R_0^2} (\vec{R}^2 - R_0^2)^2, \\ \mathcal{H}_{rel} &= \frac{\vec{p}_{rel}^2}{2\mu} + \frac{\mu}{2} \frac{(m_h^* \omega_e^2 + m_e^* \omega_h^2)}{M^3 R_0^2} r^4 - \mu\omega_{rel}^2 r^2 \\ &\quad - \frac{e^2}{4\pi\epsilon_0\epsilon_r r}, \\ \mathcal{H}_{mix} &= -2\mu(\omega_e^2 - \omega_h^2) \left( \vec{R} \cdot \vec{r} - \frac{\vec{R}^3 \cdot \vec{r}}{R_0^2} \right) \end{aligned}$$

$$\begin{aligned}
& + \frac{\mu\omega_{rel}^2}{R_0^2} \left[ R^2 r^2 + 2 \left( \vec{\mathbf{R}} \cdot \vec{\mathbf{r}} \right)^2 \right] \\
& + 2\mu \frac{(m_h^{*2}\omega_e^2 - m_e^{*2}\omega_h^2)}{M^2 R_0^2} \vec{\mathbf{R}} \cdot \vec{\mathbf{r}}^3, \quad (2)
\end{aligned}$$

where  $\mu = \frac{m_e^* m_h^*}{M}$  is the electron-hole reduced mass and  $M = m_e^* + m_h^*$  is the total mass. We have also introduced a center-of-mass frequency  $\omega_{cm} = \sqrt{\frac{m_e^* \omega_e^2 + m_h^* \omega_h^2}{M}}$  and a relative frequency  $\omega_{rel} = \sqrt{\frac{m_h^* \omega_e^2 + m_e^* \omega_h^2}{M}}$ .

The main purpose in the change of variable above is to use the solutions of  $H_{cm}$  and  $H_{rel}$  as a basis for solving the full Hamiltonian. Those solutions, *i.e.*, labeled by  $\psi_\lambda^{cm}(\vec{\mathbf{R}})$  and  $\psi_{\lambda'}^{rel}(\vec{\mathbf{r}})$ , can be solved by the series expansion method [24,25]. Here,  $\lambda = \{n_{cm}, l_{cm}\}$  and  $\lambda' = \{n_{rel}, l_{rel}\}$  represent the quantum number pair of the radial quantum number  $n$  and orbital angular-momentum quantum number  $l$ . Another advantage coming from center-of-mass and relative separation is that we can include the negative Coulomb interaction  $-\frac{e^2}{4\pi\epsilon_0\epsilon_r r}$  in  $H_{rel}$ , thus avoiding the well-known poor-convergence of the parabolic basis when the characteristic system scale is beyond the effective Bohr radius [11,26]. We now search for the wave functions of the exciton in the form

$$\Psi = \sum_{\lambda, \lambda'} A_{\lambda, \lambda'} \psi_\lambda^{cm}(\vec{\mathbf{R}}) \psi_{\lambda'}^{rel}(\vec{\mathbf{r}}). \quad (3)$$

Due to the cylindrical symmetry of the problem, the exciton wave functions can be labeled by the total orbital angular momentum  $L = l_{cm} + l_{rel}$ . To obtain the coefficients  $A_{\lambda, \lambda'}$ , the total Hamiltonian is diagonalized in the space spanned by the product states  $\psi_\lambda^{cm}(\vec{\mathbf{R}}) \psi_{\lambda'}^{rel}(\vec{\mathbf{r}})$ . In the present calculations, we first solve the single particle problem of center-of-mass and relative Hamiltonians  $H_{cm}$  and  $H_{rel}$ , keep several hundreds of the single particle states, and then pick up the low-lying energy levels to construct several thousands of product states. Note that our numerical diagonalization scheme is very efficient and essentially exact in the sense that the accuracy can be improved as required by increasing the total number of selected product states.

Once the coefficients  $A_{\lambda, \lambda'}$  are obtained, one can calculate directly the measurable properties, such as the linear optical susceptibility of the nano-rings, whose imaginary part is related to the absorption intensity measured by optical emission. In theory, the linear optical susceptibility is proportional to the dipole matrix elements between one electron-hole pair  $m$  state and the vacuum state, which in turn is proportional to the oscillator strengths  $F_m$ . In the dipole approximation, it is given by [12,26,27]

$$F_m = \left| \int \int d\vec{\mathbf{R}} d\vec{\mathbf{r}} \Psi(\vec{\mathbf{R}}, \vec{\mathbf{r}}) \delta(\vec{\mathbf{r}}) \right|^2$$

$$= \left| \sum_{\lambda, \lambda'} A_{\lambda, \lambda'} \psi_{\lambda'}^{rel}(\mathbf{0}) \int d\vec{\mathbf{R}} \psi_\lambda^{cm}(\vec{\mathbf{R}}) \right|^2, \quad (4)$$

where the factor  $\psi_{\lambda'}^{rel}(\mathbf{0})$  and the integral over  $\vec{\mathbf{R}}$  ensure that only the excitons with  $L = 0$  are created by absorbing photons. Therefore, the frequency dependence of the linear optical susceptibility  $\chi(\omega)$  can be expressed as [12,26,27]

$$\chi(\omega) \propto \sum_m \frac{F_m}{\hbar\omega - E_g - E_m - i\Gamma}, \quad (5)$$

where  $E_g$  and  $E_m$  are the respective semiconducting band gap of InGaAs and energy levels of the exciton, and  $\Gamma$  has been introduced as a phenomenological broadening parameter.

In what follows we constraint ourselves in the subspace  $L = 0$ , the most interesting case, throughout the whole calculations. As an interesting example of a typical system, we have taken the parameters  $m_e^* = 0.067m_e$ , the effective mass of the heavy hole  $m_h^* = 0.335m_e$  ( $m_e$  is the bare mass of single electron) and  $\epsilon_r = 12.4$ , which are relevant to InGaAs material [2,20,22]. The electron and hole are considered to be confined under the same potential barrier, *i.e.*,  $m_e^* \omega_e^2 = m_h^* \omega_h^2$ . If we choose the characteristic energy and length scale to be the effective Rydberg  $R_y^* = \frac{m_e^* e^4}{2\hbar^2 (4\pi\epsilon_0\epsilon_r)^2}$  and the effective Bohr radius  $a_B^* = \frac{4\pi\epsilon_0\epsilon_r \hbar^2}{\mu e^2}$ , we find that  $R_y^* = 5.0$  meV and  $a_B^* = 11.8$  nm. In the following, we perform the calculations for two ring radii: 10 and 30 nm. The ring width can be tuned by the confining potential, *i.e.*,  $W = 10$  nm corresponds to  $\hbar\omega_e = 15$  meV.

Fig. 2 displays the exciton binding energies obtained for different ring radii:  $R_0 = 10$  nm and 30 nm, as a function of nano-ring width. For comparison, the binding energy of a quantum dot with a parabolic potential  $U(\vec{\mathbf{r}}) = \frac{1}{2} m^* \omega_0^2 r^2$  is also presented in dashed line (For quantum dots,  $2W = 2\sqrt{\frac{\hbar}{m^* \omega_0}}$  is the diameter). Notice that  $E_b = E_{e-h}^0 - E_{grnd}^{ex}$ , where the first term refers to only the confinement ground state of the electron and hole, ignoring the Coulomb interaction. It is obvious that for relatively large widths, the exciton binding energy for small radius nano-rings is larger than for the large radius ones, as expected. This difference is a reflection of the strong quantum confinement in small nano-rings. As the ring width decreases, the binding energy for nano-rings with a large radius increases rapidly. For widths less than  $\approx 11$  nm, however, the two solid curves cross and their sequence is reversed. This crossover is caused by the strong anisotropic confinement in nano-rings: For smaller ring widths, the resulting exciton wavefunctions are increasingly elongated along the ring, and thus the exciton is confined in a quasi one-dimensional system with a characteristic size  $\approx W$ . On the other hand, by decreasing the ring radius in a fixed potential strength (or

a fixed ring width), nano-rings can be tuned from quasi one-dimensional to two-dimensional systems. In other words, nano-rings would behave like quantum dots when their radii are comparable to widths (see Fig. (1a)). One thus can expect that with a fixed sufficient small ring width, the effective size of the exciton might be smaller for a larger ring radius, and in turn causes the enhancement of its binding energy.

Another feature shown in Fig. 2 is the similarity of the curves for the large radius nano-ring and the quantum dot. This is due to the comparable confinement area of the two systems, as pointed out by Song and Ulloa that the excitons in nano-rings behave to a great extent as those in quantum dots of similar dimensions [11]. It is also important to emphasize that for a nano-ring with a large ring radius and ring width, the binding energy approaches approximately the exact result of a free two-dimensional exciton, *i.e.*,  $E_b = 4R_y^* = 20$  meV.

Fig. 3 shows the exciton oscillator strengths versus the ring width, for two ring radii (two solid lines) and a quantum dot with a parabolic potential (the dashed line). It is readily seen that the oscillator strength of the large radius nano-ring is much larger than that of the small radius nano-ring in the whole range of widths shown, which is also an indication of the strong quantum confinement in small nano-rings, as mentioned above. For a larger ring width, the oscillator strengths of the two nano-rings clearly increase, but not as fast as that of the quantum dot.

To support the experimental relevance of our results, we have also calculated the linear optical susceptibility of nano-rings. Figs.(4a) and (4b) show the typical results for different values of the ring width and two ring radii, where a broadening parameter  $\Gamma = 0.5$  meV is used. Those curves represent all the possible transitions of excitonic states which would be measurable via photoluminescence excitation measurements (PLE). In contrast to the conventional quantum dots, in which the low-lying exciton state transitions have the same amplitudes and are nearly equally distributed (a reflection of excitations of the center-of-mass degree of freedom), the low-lying transitions of nano-rings show a rapid dampen with frequency and their positions are not periodic. This difference is a reflection of the anisotropic confinement of nano-rings: Since the exciton is confined in a quasi one-dimensional system, its center-of-mass degree of freedom is greatly suppressed and its relative motion becomes dominant, thus resulting the destruction of the regular patterns observed in quantum dots. Note that this behavior is indeed observed in a recent experiment [3]. Another noticeable feature in Figs. (4a) and (4b) is that those transition peaks are strongly red shifted as the ring width increases, indicating the less confinement for larger ring widths.

In conclusion, we have shown the strong quantum confinement effects on excitons in a nano-ring based on a simple model Hamiltonian. By numerical diagonalization, we calculate the binding energies, oscillator

strengths and their dependence on the width of nano-rings, as well as the linear optical susceptibility. The anisotropic confinement in nano-rings is clearly demonstrated, which can be confirmed by future measurements of optical emission on InGaAs nano-rings with tunable sizes.

#### Acknowledgments

The financial support from NSF-China (Grant No. 19974019) and China's "973" program is gratefully acknowledged.

- 
- [1] R. J. Warburton, C. Schäflein, D. Haft, F. Bickel, A. Lorke, K. Karra, J. M. Garcia, W. Schoenfeld, and P. M. Petroff, *Nature* **405**, 926 (2000).
  - [2] A. Lorke, R. J. Luyken, A. O. Govorov, J. P. Kotthaus, J. M. Garcia, and P. M. Petroff, *Phys. Rev. Lett.* **84**, 2223 (2000).
  - [3] H. Pettersson, R. J. Warburton, A. Lorke, K. Karrai, J. P. Kotthaus, J. M. Garcia, and P. M. Petroff, *Physica E* **6**, 510 (2000).
  - [4] A. Lorke and R. J. Luyken, *Physica B* **256**, 424 (1998).
  - [5] A. Lorke, R. J. Luyken, M. Fricke, J. P. Kotthaus, G. Medeiros-Ribeiro, J. M. Garcia, and P. M. Petroff, *Microelectronic Engineering* **47**, 95 (1999).
  - [6] D. Mailly, C. Chapelier, and A. Benoit, *Phys. Rev. Lett.* **70**, 2020 (1993).
  - [7] L. Wendler and V. M. Fomin, *Phys. Rev. B* **51**, 17814 (1995).
  - [8] A. Chaplik, *JETP Lett.* **62**, 900 (1995).
  - [9] V. Halonen, P. Pietiläinen, and T. Chakraborty, *Europhys. Lett.* **33**, 377 (1996).
  - [10] R. A. Römer and M. E. Raikh, *arXiv:cond-mat* **9906314** (1999).
  - [11] J. Song and S. E. Ulloa, *arXiv:cond-mat* **0008407** (2000).
  - [12] W. Que, *Phys. Rev. B* **45**, 11036 (1992).
  - [13] V. Halonen, T. Chakraborty, and P. Pietiläinen, *Phys. Rev. B* **45**, 5980 (1992).
  - [14] J. Song and S. E. Ulloa, *Phys. Rev. B* **52**, 9015 (1995).
  - [15] T. Uozumi, Y. Kayanuma, K. Yamanaka, K. Edamatsu, and T. Itoh, *Phys. Rev. B* **59**, 9826 (1999).
  - [16] L. Jacak, P. Hawrylak, and A. Wójs, *Quantum Dots* (Springer-Verlag, Berlin Heidelberg, 1998), and references therein.
  - [17] T. Chakraborty and P. Pietiläinen, *Phys. Rev. B* **50**, 8460 (1994).
  - [18] V. Gudmundsson and Á. Loftsdóttir, *Phys. Rev. B* **50**, 17433 (1994).
  - [19] L. Wendler, V. M. Fomin, A. V. Chaplik, and A. O. Govorov, *Phys. Rev. B* **54**, 4794 (1996).
  - [20] A. Emperador, M. Pi, M. Barranco, and A. Lorke, *Phys. Rev. B* **62**, 4573 (2000).
  - [21] M. Koskinen, M. Manninen, B. Mottelson, and S. Reimann, *arXiv:cond-mat* **004095** (2000).

- [22] H. Hu, J. -L. Zhu, and J. J. Xiong, arXiv:cond-mat **0005520** (2000).
- [23] P. Borrmann and J. Harting, arXiv:cond-mat **0008464** (2000).
- [24] J. -L. Zhu, J. J. Xiong, and B. -L. Gu, Phys. Rev. B **41**, 6001 (1990).
- [25] J. -L. Zhu, Z. Q. Li, J. Z. Yu, K. Ohno, and Y. Kawazoe, Phys. Rev. B **55**, 1 (1997).
- [26] J. Song and S. E. Ulloa, Phys. Rev. B **52**, 9015 (1995).
- [27] G. W. Bryant, Phys. Rev. B **37**, 8763 (1988).

### Figures Captions

Fig.1. The confining potential  $U(\vec{r}) = \frac{m_e^* \omega_e^2}{2R_0^2} (\vec{r}^2 - R_0^2)^2$  with different ring radii  $R_0$ : 10 nm (a) and 30 nm (b). The solid and dashed lines correspond to the ring width  $W = 16.7$  and  $9.6$  nm, respectively.

Fig.2. The exciton binding energies for the nano-ring as a function of ring width with two different ring radii  $R_0 = 10$  and  $30$  nm. For comparison, the result for a parabolic quantum dot is also displayed in dashed line.

Fig.3. The exciton oscillator strengths versus the ring width, for two ring radii (two solid lines) and a quantum dot with a parabolic potential (the dashed line).

Fig.4. Imaginary part of linear optical susceptibility as a function of frequency  $\omega$  for different values of the ring width and two different ring radii  $R_0 = 10$  nm (a) and  $R_0 = 30$  nm (b). In each panel, from bottom to top, the ring widths are 10, 15, 20 and 25 nm. For clarity, the semiconducting band gap  $E_g$  is set to be zero.

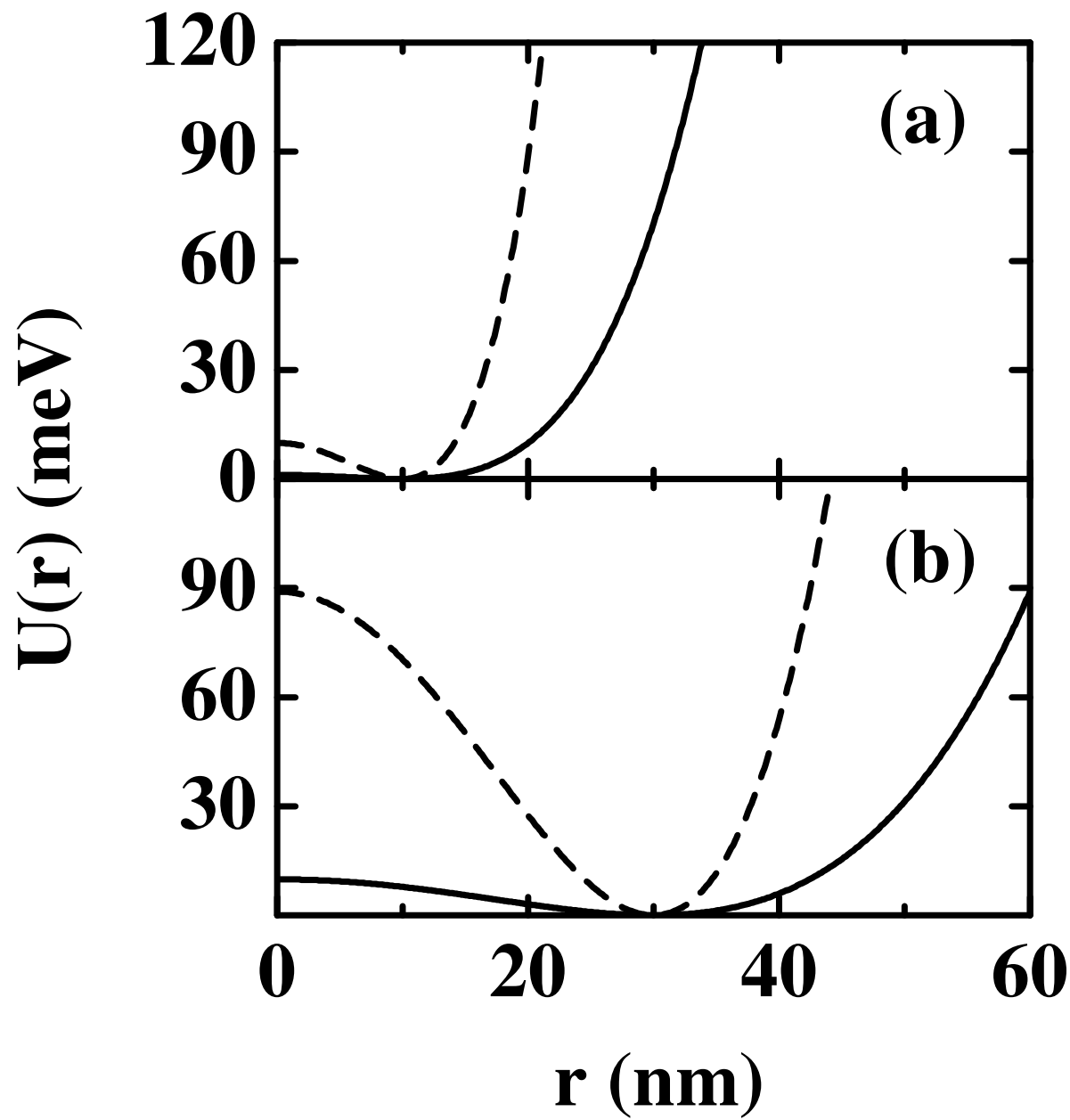


Fig. 1  
Size effects on exctions.....  
H. Hu *et al.*

**Fig. 1**



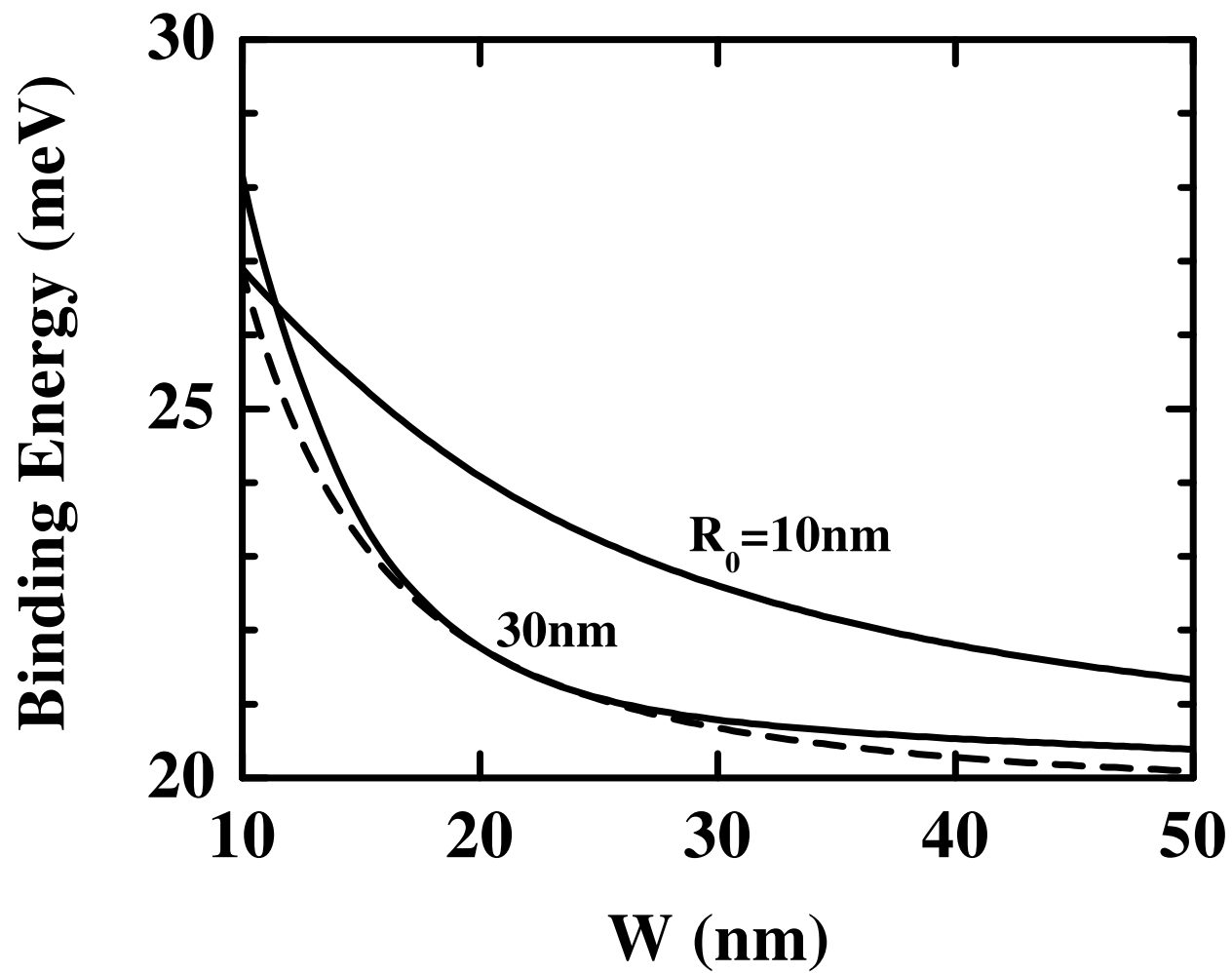


Fig. 2  
Size effects on exctions.....  
H. Hu *et al.*

**Fig. 2**



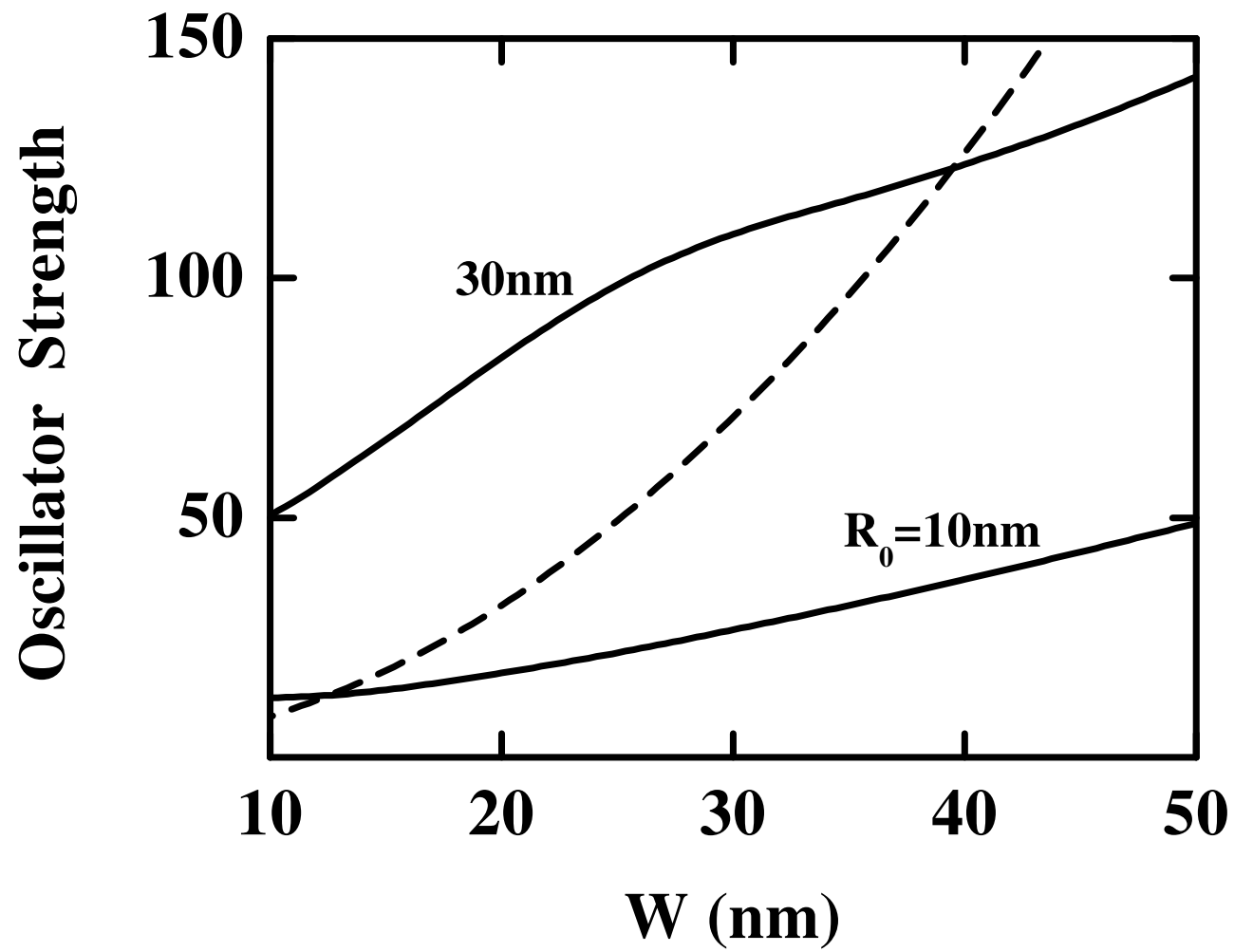


Fig. 3  
Size effects on exctions.....  
H. Hu *et al.*

**Fig. 3**



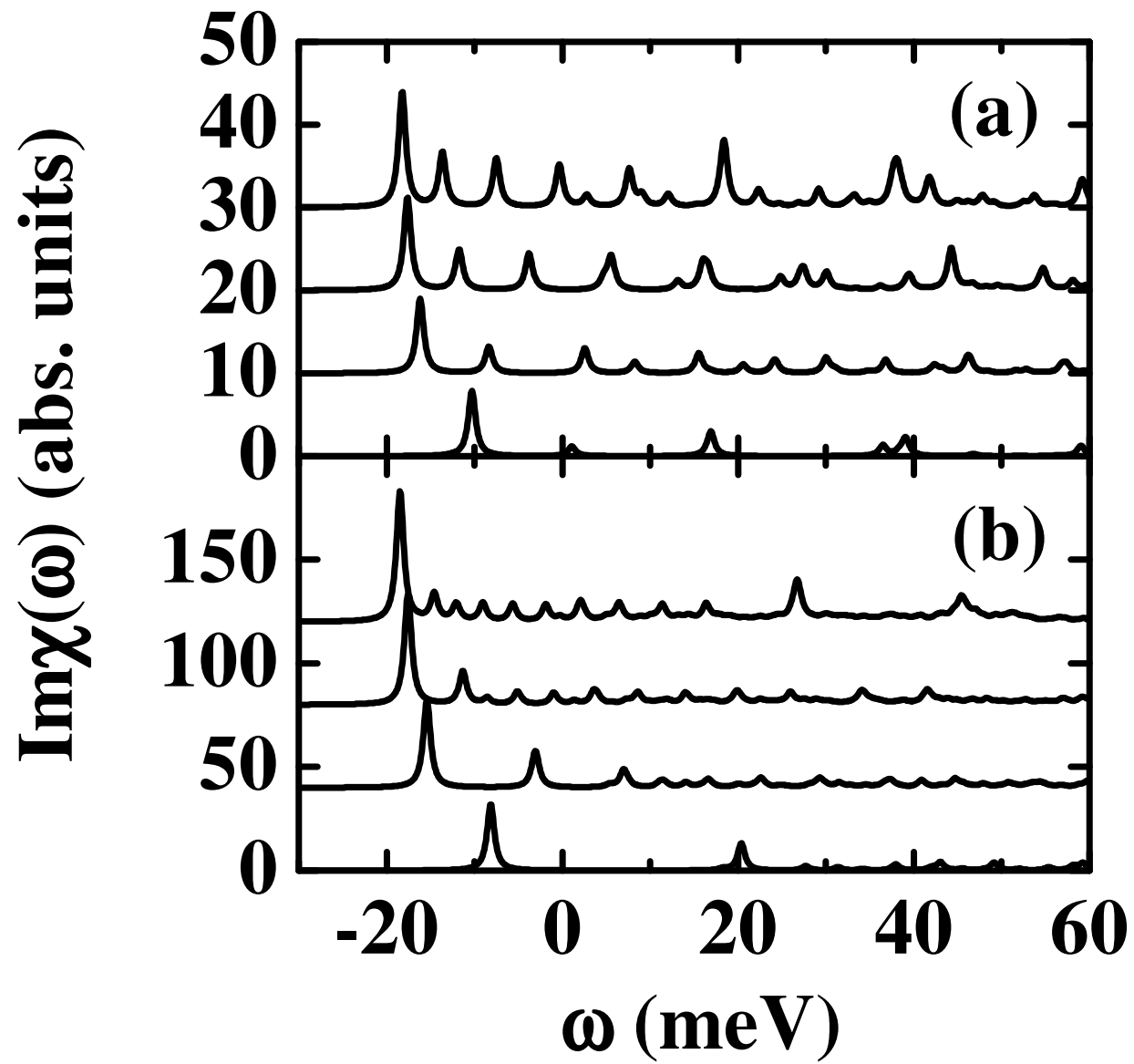


Fig. 4  
Size effects on exctions....  
H. Hu *et al.*

**Fig. 4**

